Arch. Bas. App. Med.13 (2025) 80-90
www.archivesbamui.com
www.ojshostng.com/index.php/abam

Research Article

Mushroom-Mediated Synthesis of Ag, Fe, and Ag-Fe Nanoparticles of *Pleorotus ostreatus*: Surface Characterization and Antimicrobial Activity

***Fadare D. A.[1], Yussuf L. A.[2], Oladokun M. S.[1], Ogunsile B. O[2].**
[1]*Department of Chemical Sciences, Anchor University, Lagos, Nigeria.*
[2]*Department of Chemistry, University of Ibadan, Ibadan, Nigeria*
Accepted: October 21, 2025

Abstract
Conventional methods for nanoparticle synthesis are often associated with environmental pollution, underscoring the need for safer, more eco-friendly alternatives. Plants and fungi-mediated synthesis offer a green chemistry approach by harnessing natural biological systems for nanomaterial production. In this study, *Pleurotus ostreatus* (Oyster mushroom) extract was employed as a reducing and capping agent for the synthesis of Ag (silver), Fe (Iron), and Ag-Fe (silver-iron) bimetallic nanoparticles. The synthesis was optimised by varying reaction parameters, and the nanoparticles were characterised using UV-visible and FTIR spectroscopy, scanning electron microscopy and X-ray diffraction (XRD), which confirmed particle sizes ranging from 2-46.7 mm with spherical, triangular and rod-shaped morphologies and crystalline structures. The antimicrobial activities of the nanoparticles were assessed against bacterial and fungal strains, revealing dose-dependent inhibitory effects across all tested microorganisms. These findings demonstrate that *Pleurotus ostreatus*-mediated synthesis provides a sustainable route for producing mono and bimetallic nanoparticles with promising antimicrobial potential.

Key Words: *Metallic nanoparticles, Pleurotus ostreatus, biosynthesis, antimicrobial activity, operational variables*

INTRODUCTION

Nanoparticles are defined as nano-objects of sizes ranging between 1 to 100 nm with all external magnitudes in the nano-measure, where the lengths of the longest and the shortest axes do not differ significantly (Nadeem and Dirk, 2022). Nanoparticles have different shapes, sizes, and structures, which influence their physical and chemical properties and, hence, their biocompatibility.

The distinct characteristics of nanomaterials, compared with their macroscale counterparts, make them an important material for various applications.

The use of chemical and physical synthesis methods for nanoparticles has raised significant concerns due to toxic byproducts. Research has focused more on green synthesis of nanoparticles as it offers an environmentally benign alternative to chemical and physical methods. Major advantages of green synthesis include being cost-effective, environmentally friendly, easily scaled up for large-scale synthesis, and requiring minimal pressure, energy, temperature, and toxic chemicals (Guor and Fain, 2019; Ying *et al*., 2022).

Studies on the synthesis of metal and metal-oxide nanoparticles (Gd, Ag, Pt, etc.) using plant extracts have been reported (Ejidike *et al*., 2024; Francis *et al*., 2023; Hancharova *et al*., 2024). Interest in the production of nanoparticles using edible and medicinal mushrooms has increased because these macrofungi act as eco-friendly bioworkshops that secrete large quantities of extracellular proteins and enzymes, which are necessary for the reduction of metal ions to their zerovalent or nanoform states. Additionally, the nanoparticles synthesised using mushrooms exhibit higher stability, longer shelf life, enhanced biological activity, high yield, and ease of handling. Although the mechanism of synthesis is still not fully understood, several studies propose that fungal reductases and flavins are a major factor in the synthesis pathway. A selection of macrofungi has been used for the synthesis of monometallic and bimetallic nanoparticles with metals such as Au, Ag, Fe, Pt, and Ag-Fe (Baasher *et al*., 2023; Alavi & Ashengroph, 2023)

A bimetallic nanoparticle is a combination of two different metals that exhibit several new and improved properties, and as such, is preferred over monometallic nanoparticles (Mela *et al*., 2022). The use of multiple metals in the synthesis of nanoparticles exhibited synergistic effects, including antimicrobial activity. Therefore, interactions among metal groups are explored in the synthesis and design of bimetallic nanoparticles, leading to the development of more efficient combinatorial antimicrobials composed of synergistic metals. Bimetallic nanoparticles have emerged as noteworthy entities in recent years due to their unique optical, electronic, magnetic, and catalytic properties (Kumar *et al*., 2024). Combining two different metal elements yields diverse morphologies and structures, as well as distinct mechanisms of action and a reduced likelihood of resistance development (Ribeiro *et al*., 2022). Studies have shown that bimetallic nanoparticles, more than their counterpart, exhibit new and improved properties both in antimicrobial and catalytic

**Author for Correspondence:* Tel: +234 7089052710 E-mail: *dfadare@aul.edu.ng*

activities; hence, bimetallic nanoparticles such as Fe/Ru, Ag−Pd, Ag–Fe bimetallic nanoparticles, among many others, have been synthesised and put to applications.

Iron nanoparticles (FeNPs) have gained much interest because of the magnetic, catalytic, and remediation properties, which allow their suitability for a wide range of applications, including their use as catalysts, drug delivery systems, sensors, water purification, environmental remediation and energy storage (photovoltaic and solar cells) and conversion. FeNPs are used as contrast agents to enhance tissue and organ visualisation in magnetic resonance imaging. They are valuable in magnetic recording media, e.g., hard disk drives (Zhuang and Gentry, 2011).

Research has predominantly focused on prokaryotes for synthesizing metallic nanoparticles due to several factors. Bacteria are abundant, adaptable to extreme conditions, cost-effective to cultivate, and easily controlled in terms of growth parameters such as temperature, oxygenation, and incubation time. However, fungi are of greater interest than bacteria for nanoparticle synthesis due to their secretion of higher amounts of proteins, which enhance the production of metallic nanoparticles (Saravanan *et al*., 2021). Furthermore, fungi offer ease of scale-up and downstream processing, contributing to cost-effectiveness. Similar studies reported the biological synthesis of nanoparticles using *Garnoderma lucidum*, which was used to design silver nanoparticles on cotton fabric and serves as an antimicrobial dressing material that can be stabilised by proteins or other bioactive compounds (Paul *et al*., 2015). FeNPs were also synthesised by employing Alternaria alternate fungus through the reduction of aqueous Fe^{3+} under dark conditions (Mohamed *et al*., 2015).

Mushroom is the fruiting body of a macro-fungus in the kingdom Myceteae. They are either produced above ground (epigeous) or underground (hypogeous), visible to the naked eye and can be picked by hand. *Pleurotus ostreatus*, a member of the family Pleurotaceae, is a common edible mushroom and is commonly referred to as the oyster mushroom. However, to differentiate it from others, its mycelium is pure white. Minimal mushroom production worldwide poses a major threat to the availability of biomass needed to produce reducing agents that are safer for medical consumption; hence the need for optimisation of mushroom production to generate sufficient biomass for a sustainable process and high-quality metallic nanoparticles (Deepalakshmi & Sankaran, 2014).

The escalating threat of drug-resistant infections is a major global health challenge with alarming projections of over ten million annual deaths from drug-resistant infections by 2050 (Rawson *et al*., 2020). Metal nanoparticles offer promising avenues as antimicrobial, medicinal, and anti-infective agents. Noble metal nanoparticles such as silver and gold exhibit potent and enduring antibacterial activity against a wide range of microorganisms, with applications in medical devices, food preservation, dental materials, cosmetics, and other healthcare products. Reactions are also controlled by pH and temperature; thereby, nanoparticle parameters, e.g., size and shape, can be adjusted. The shape, size, structure, stability, chemical composition, crystallinity, and surface interaction of nanoparticles are key factors in determining the behaviour, characteristics and properties of nanomaterials.

The work explored various combinations of substrates and supplements to optimise mushroom yield (biomass availability) for sustainable nanoparticle synthesis via a green route. The effects of operational variables such as time, concentration, ratio of extract to precursor and pH on the synthesis of nanoparticles was determined. Antimicrobial activities of synthesised monometallic and bimetallic nanoparticles were also determined.

MATERIALS AND METHODS

Silver nitrate ($AgNO_3$), Sodium hydroxide (NaOH), and Iron (III) nitrate ($Fe(NO_3)_3 \cdot 9H_2O$) were purchased from JHD, China. All reagents were used as received, and double-distilled water was used to prepare the standard stock solution.

Oyster mushroom white strain spawn was purchased from the Mycology laboratory of the Department of Botany, University of Ibadan, Nigeria. The two major substrates, *Anogeissus leocarpus* sawdust, and corncobs were got from a local in Ibadan, Nigeria while the wheat bran, lime and sugar were purchased from a local market in Ibadan, Nigeria

Method

Experimental Site and Design: The study (substrate optimisation for *Pleurotus ostreatus* production) was conducted in accordance with the procedure of Wilson and Del Rosario (2020). The mushroom incubation was carried out in an improvised wooden chamber that also served as a growing room in the well-aerated laboratory. There were 24 experimental units, consisting of 8 treatments and 3 replicates. The major substrates used for the culturing of white oyster mushrooms were lignocellulosic wastes of wood sawdust (Anogeissus leocarpus) and corncobs with different combination treatments, while nutritional supplements (wheat bran, agricultural lime -$CaCO_3$ and Sugar) serve as additives.

Substrate, Fruiting Bags Preparation, Supplementation

Clean, new corn cobs were crushed with a chopper to produce cobs approximately 0.5 cm in size (Rambey *et al*., 2019). Mushrooms were produced as described by Oseni *et al*., (2012). Major substrates (sawdust and corn cobs) were thoroughly and appropriately mixed with the additives on a plastic sheet before adding 70 % water, as shown below (Itelima, 2010). The media were properly mixed until the water was absorbed (Noor *et al*., 2023).

Compost 1 (Oseni *et al*., 2012).

Tc1 =100 % sawdust substrate + 0 % Additive (0% wheat bran + 0% lime) -Control

T1= 95 % sawdust substrate + 5 % Additive (3% wheat bran + 2% lime)

T2= 90 % sawdust substrate + 10 %Additive (6 % wheat bran + 4 % lime)

T3= 80 % fermented sawdust substrate + 20 % Additive (12 % wheat bran + 8 %lime)

Compost 2 (Oei, 2005).

Tc2 =100 % corncob substrate + 0 % Additive (wheat bran-0% + lime 0%) -Control

T4= (73 % sawdust + 25 % corncob) substrate + 2 %Additive (lime)

T5= 94% sawdust substrate +6 %Additive (wheat bran-5% + lime-1%)

T6 = 94% corncob substrate +6 %Additive (wheat bran-5% + lime-1%)

Difference (sawdust and sorn cob)

Compost 3 (Fasidi *et al*., 2008)

T7 = 78% sawdust substrate + 22% Additive (wheat bran-20% + lime-1%+ sugar-1%)

T8 = 78% corncob substrate + 22% Additive (wheat bran-20% + lime-1%+ sugar-1%) (different substrate)

Five hundred grams of each mixed substrate were filled in heat-resistant polythene fruiting bags (20 cm x 35cm) and sealed using a cotton-plugged polyvinyl chloride pipe ring and a rubber band.

Heat Treatment: This was done by sterilisation at 100 °C using a 12-inch pressure pot. A wooden rack is placed on the bottom of the pot. The pot is filled with water to a height of 3 inches. The bags with the substrate are placed on the rack inside the oil drum. The lid is put on the pot and steamed (100°C) for 8 hours by heating the pot. The sterilised substrates were allowed to cool to room temperature (28-32 °C for 12 hours (Keziah *et al*., 2022).

Inoculations/spawning: 70 % ethanol was used to sterilise surfaces in the inoculation chamber. A sterilised spatula was used to loosen the colonised bird seeds in the stock spawn bottles. The sterilised substrate bags were spawned by opening them and adding 50g of spawn (10%) (Fikre, 2012) while the ethanol lamp was lit.

Incubation and Spawn running (Ramification): The inoculated bags were kept upright inside an improvised incubation chamber, a room to let the mushroom mycelium grow for 25 - 45days under limited light and relative humidity between 85-90%. The mycelia had fully colonised about 70% of the bags within 30 days.

Fruiting and Harvesting: The bags were opened immediately after the mycelium had fully covered the substrate, by removing the cotton plugs, and the plastic tops of the bags were carefully cut away to avoid damaging the mycelium. Exposing a larger surface to the open air produces small mushrooms. The polythene bags were then cut open to expose strips of the saw dust and corn cobs to give room for normal shape fruit bodies. Mature mushrooms were harvested manually in a single flush. The high humidity was maintained throughout the experiment.

Green Synthesis

Collection and Preparation of Crude Extract of *Pleurotus ostreatus*: Fruiting bodies of *Pleurotus ostreatus* produced as above were collected from T4, which ranked first, and thoroughly washed with distilled water and finely cut into small pieces. 200 g of fresh mushrooms was added to 1000 mL of distilled water, heated for 1 hour in a water bath at 60 °C, and filtered through Whatman No. 1 filter paper.

Preparation of Standard Stock Solutions of Precursor Salts ($AgNO_3$ and $Fe(NO_3)_3$): 500 mL of 1 mM, 2 mM and 3 mM of $AgNO_3$ solutions were prepared by dissolving 0.085 g ,0.17g and 0.255 g of anhydrous $AgNO_3$ crystalline salt each in 500 mL of distilled water respectively.

$Fe(NO_3)_3$) (1 mM, 2 mM and 3 mM) solutions were prepared by dissolving 0.202 g, 0.404 g, and 0.606 g of the hydrated $Fe(NO_3)_3).9H_2O$ salt each in 500 mL of distilled water respectively.

Optimization of Biosynthesis of Silver Nanoparticles (AgNPs), Iron Nanoparticles (FeNPs): The effects of various operational parameters (time, concentrations, ratios and pH) on the synthesis of the metal nanoparticles were determined as previously describe as follows (Ogunsile *et al*., 2023). 50 mL of freshly prepared *P. ostreatus* extract was added to 50 mL $AgNO_3$ (1 Mm) salt solution as a reducing, capping and stabilizing agent at 60ºC with continuous stirring for 60 minutes (Manikanda and Ramansubu, 2021).

The effect of time (t): the extract and salt solution samples were measured for absorbance at 0, 10, 20, 30, 40, and 60-minute intervals during synthesis. The effect of concentration of precursor salt solution was investigated by reducing 50 ml of 2 mM and 3 mM of $AgNO_3$ each with 50 mL of the PO extract (1:1) at 60ºC for 60 mins.

The effect of the ratio of extract (reducing agent) to precursor salt solution was equally examined by reducing the 2 mM of $AgNO_3$ salt solution with PO extract using a ratio of 1:2 and then a ratio of 1:3.

The reduction of $AgNO_3$ to Ag nanoparticles was indicated by the colour change from pale yellow to reddish brown.

The same procedures were carried out for the synthesis of iron nanoparticles using $Fe(NO_3)_3$ but with a slight difference in the time interval i.e 0, 5, 10, 15, 20, 40 and 60 mins. The reaction was monitored by a colour change from light brown to dark brown. The solution of AgNPs and FeNPs were separately centrifuged, supernatant decanted and oven dried at 60ºC.

The effect of concentration of salt solution was investigated by reducing 50 mL of 2 mM and 3 mM of $AgNO_3$ each with 50 mL of the PO extract (1:1) at 60 ºC for 60 mins.

The effect of ratio of extract (reducing agent) was examined by reducing the 2 Mm of $AgNO_3$ salt solution with PO extract first in ratio 1:2 and then ratio 1:3.

Variation of pH: The pH of the extract was measured and found acidic (3.77), adjusted to a neutral pH by adding some drops of 0.125 M of aqueous NaOH. 10 mL of the neutral solution was heated at 60ºC for 60 min and the remaining

volume was made alkaline (pH 9.00) by addition of few drops of 0.125 M of aqueous NaOH and heated at 60ºC for 60 min.

Characterization of AgNPs, FeNPs and Ag-Fe BNPs

a. UV -Visible Spectroscopic Analysis: All the bimetallic nanoparticles solution samples prepared were analyzed on Spectroquant Pharo. 300 M spectrophotometer with 2cm quartz cuvette, 1.0 nm resolution in the range of 200 nm - 900 nm possessing a maximum scan speed of approx. 3300 nm per min.

b. Fourier Transform Infrared (FTIR) Spectroscopic Analysis: Mushroom extract (200mL) was used to prepare a solid sample for this analysis. The synthesized AgNPs, FeNPs and Ag-Fe bimetallic were completely dried at 60°C. Finally, the dried nanoparticles and the evaporated extract were analyzed by PerkinElmer FTIR Spectrometer between 4000-400 cm^{-1} to determine the ability of different biomolecules as reducing and capping /stabilizing agent in the formation of the AgNPs, FeNPs and Ag-Fe bimetallic nanoparticles.

c. Scanning Electron microscope Analysis (SEM): The morphological analysis of biosynthesized AgNPs, FeNPs and Ag-Fe bimetallic nanoparticles using SEM JEOL-JSM-7600F

d. X-ray Diffraction Analysis (XRD): The crystal structure of powdered samples of the biosynthesized AgNPs, FeNPs, Ag-FeNPs bimetallic nanoparticles were examined using pelletized material with size 0.074 mm. The samples were compacted by mildly hand pressing in an aluminum alloy grid (35 mm x 50 mm) on a flat glass plate and covered with a paper. Each sample was run through the Rigaku D/Max-lllC X-ray diffractometer (Rigaku Int. Corp. Tokyo, Japan) at scanning rate of 2 0/min in the 2 to 500 at room temperature with a CuKa radiation set at 40 kV and 20 mA. The diffraction data (d value and relative intensity) gotten was compared to that of the standard data.

Antimicrobial assay: A total of seven microorganisms which include four bacteria *Staphylococcus aureus*, *Escherichia coli*, *Pseudomonas aeruginosa*, *Klebsialla pneumonia*, and three fungi *Candida albicans*, *Aspergillus niger*, *Penicillium notatum* were used in the antimicrobial assay.

RESULTS

Substrate Optimization for Oyster Mushroom Production: Yield parameters such as mushroom yield (g) biological efficiency (%), pileus thickness and diameter (cm), number of contaminated substrates bags, number of days of full mycelia colonization, mycelia growth rate etc. were determined. (Table 1). T4, Tc1, T2, T1 and T6 were ranked 1st,2nd ,3rd, 4th and 5th respectively (Keziah *et al*., 2022). It may be suggested that sugar may not be a suitable additive for the specie of wood sawdust used as the substrate.

Table 1:
Oyster Mushroom Performance Based on Yield Parameters

Substrate Treatments	No. of Contaminated Bags	Mycelium Growth Rate at 2 weeks (%)	No of Days for Full Mycelia Colonization	Days of First Sprouting	Rank
Tc1	1	80	33	38	2
T1	Nil	80	31		4
T2	Nil	75	37	41	3
T3	Nil	10			
Tc2	1	60	40		
T4	Nil	80	30	52	1
T5	1	5			
T6	Nil	70	33		5
T7	2	0			
T8	1	20			

Figure 1:
Pleorotus ostreatus **(Oyster mushroom)**

UV Visible Absorbance Spectra of AgNPs, FeNPs, Ag-Fe BNPs and Operational Variables

Synthesis of Ag, Fe and Ag-Fe Nanoparticles: The formation of nanoparticles were indicated by various colour changes from pale yellow to reddish brown depending on the metal (Figure 2a-c). Excitation of surface plasmon resonance (SPR) in the metal nanoparticles give rise to different colour observed with increase in intensity (deep brown) with time.
During the synthesis of Ag nanoparticle the colour changed from light yellow to brown. The reduction process of metal ions (e.g. Ag+) was confirmed by UV-Vis spectroscopy which provides information about the size, aggregation and surface chemistry of *Pleurotus ostreatus* nanoparticles.
Figure 3a shows a moderately intense maximum absorption peaks in the UV-visible spectrum were observed at 248 nm and 295 nm which is not within characteristics localized surface plasmon resonance range (LSPR), 400-600 nm for

green synthesized Ag-nanoparticles i.e no SPR band was observed. This agrees with the result reported in a similar study carried out by Sneha *et al*. (2020) where the maximum absorption peak was observed at 200 nm. The synthesis of AgNPs was also confirmed by the observation an increased or higher intensity of absorption of AgNPs as compared to that of the PO in the spectrum of PO Extract and AgNPs (Figure 3a).

Dark brown coloration was obtained when *Pleurotus ostreatus* extract was added to of Ag+ and Fe+ metal ion solution (Figure 3c) indicative of formation of Ag-Fe bimetallic nanoparticles. The shell that conforms the core-shell Ag-Fe BNPs. The maximum absorption peak in the UV spectrum of Ag-Fe BNPs was observed at a wavelength of 300 nm, this closely agrees with the value reported by Padilla -Cruz *et al*.,2021, in which the absorption peak in the UV spectrum of a green synthesized Ag-Fe BNPs was observed at 290 nm.

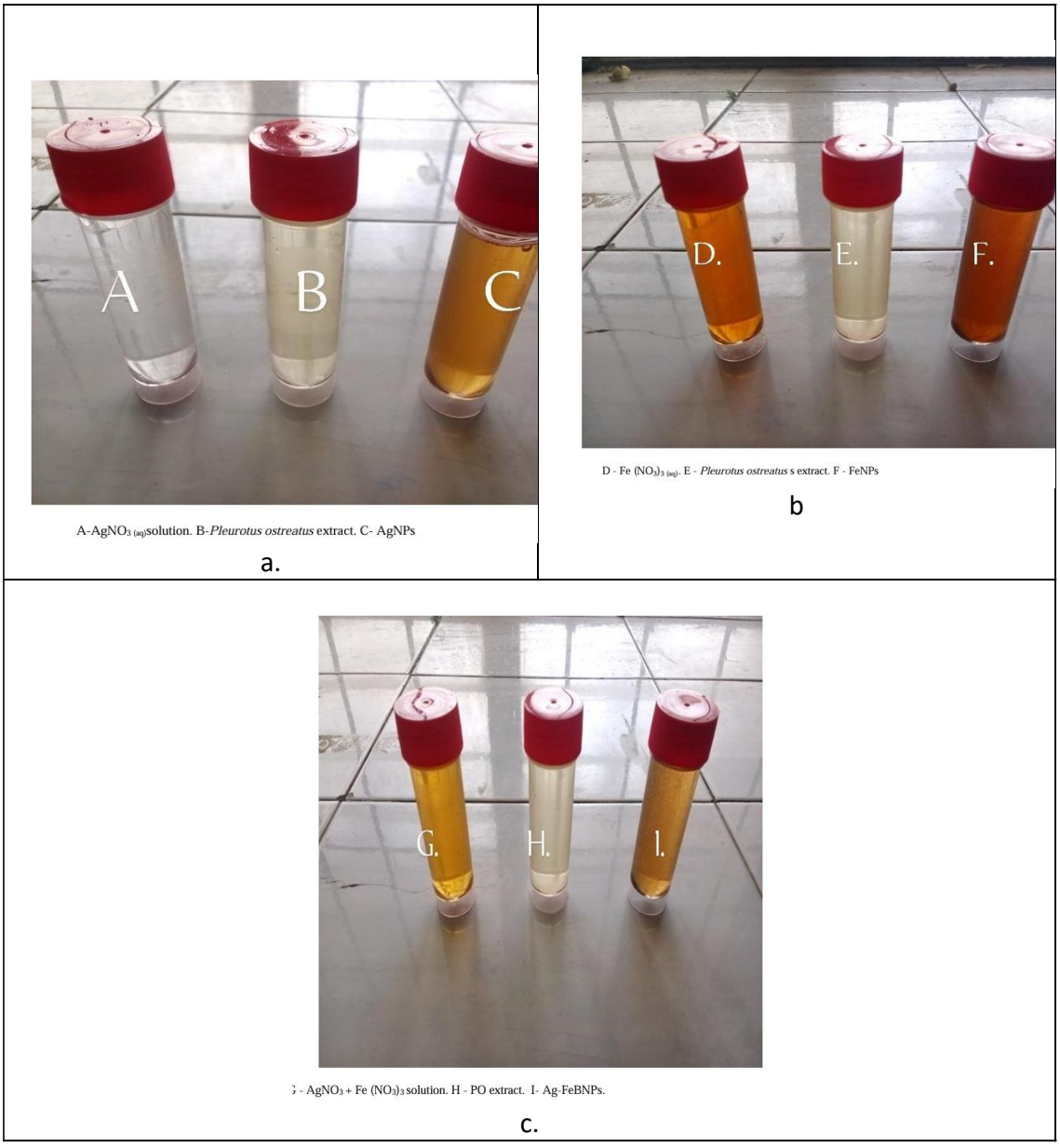

Figure 2:
Colour change during the synthesis of nanoparticles (a) AgNP (b) FeNP (c)Ag-FeNP

Operational Parameters (Ogunsile *et al*., 2024)

i). Time: The synthesis of AgNPs (silver nanoparticles) studied under some operational variables showed an increase in the time of synthesis from 0 to 60 min resulted in significant increased absorbance intensity. The synthesis of AgNPs was also suggested by the observation an increased or higher intensity of absorption of AgNPs as compared to that of the PO in the spectrum of PO Extract and AgNPs. A moderately intense maximum absorption peaks in the UV-visible spectrum were observed at 248 nm and 295 nm which is not within characteristics localized surface plasmon resonance range (LSPR), 400 nm-600 nm for green synthesized Ag-nanoparticles i.e no SPR band was observed. This agrees with the result reported in a similar study carried out by Ejidike *et al*., 2024; Sneha *et al*. 2020 where the maximum absorption peak was observed at 200 nm

The UV spectrum of FeNPs (Figure 3a) showed major absorption peaks at 248 nm and 298 nm of which the intensity increases with time, similar report was given by Mohamed *et al*., 2015 where the two maximum peaks of 238 nm and 265 nm were observed in the UV spectrum of a fungus synthesized FeNPs and the intensity of the peaks equally increase with increase in the time of synthesis from 0 to 60 min. This result also resonates with the report of a similar study carried out by

Banerjee *et al*, 2014 where two major absorption peaks, 216 nm and 268 nm observed with intensity found to increase with increase in time.

An absorption peak of higher absorbance than that of the maximum absorption peak in PO spectrum was observed at 340 nm wavelength in the UV-visible spectrum of FeNPs prepared in ratio 1:1 of 1 mM of Fe $(NO3)_3$ to PO extract indicating the synthesis of FeNPs. The intensity of the absorbance increases with increase in the time of synthesis from 0 to 60 min (Figure 3b).

Major absorption peak was observed at 296 nm wavelengths in the UV spectrum of the PO extract and Ag-Fe BNPs at 60ºC for 60 mins meanwhile the intensity of absorption peak of Ag-Fe BNPs solution was higher than that of the PO extract confirming the synthesis of silver-iron bimetallic nanoparticles.

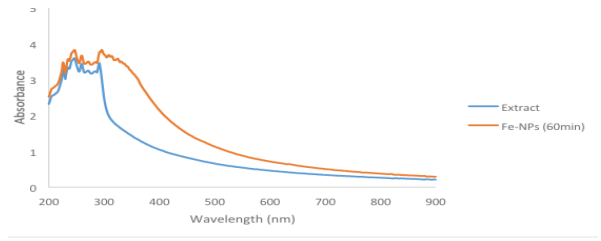

a

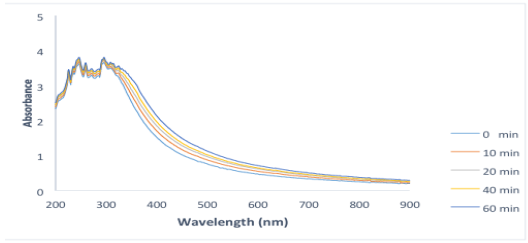

b

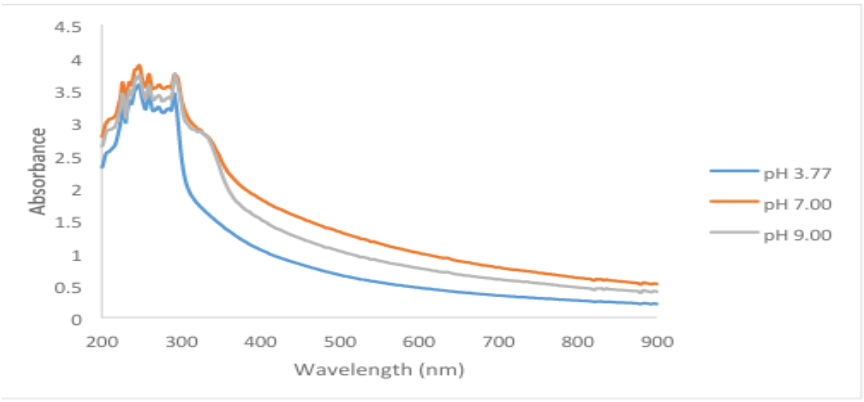

c

Fig 3:
UV of (a)FeNNP (b) effect of time and (c) Effect of pH

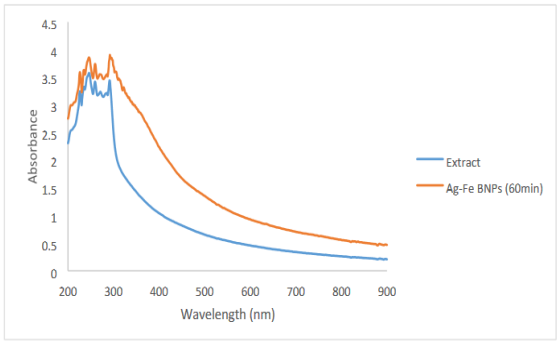

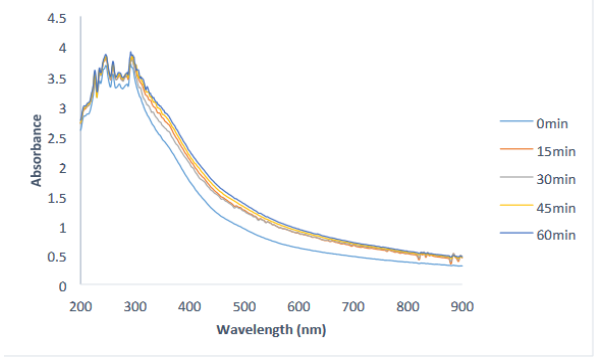

a b

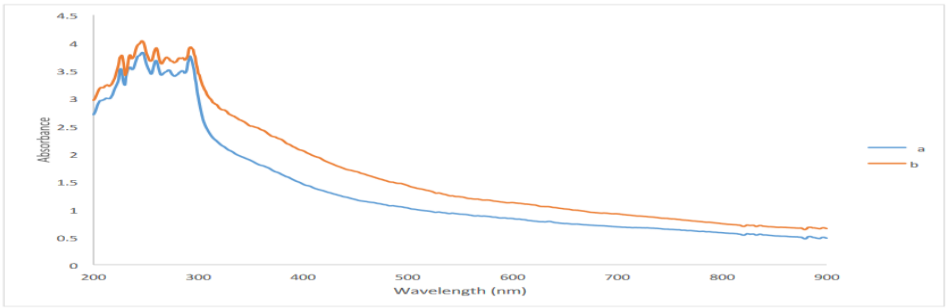

c

a - $AgNO_3$ (1mM) + $Fe(NO_3)_3$(2 mM) , b - $AgNO_3$ (2 mM) + $Fe(NO_3)_3$ (1 mM)

Figure 4:
UV Absorbance Spectrum for Ag-Fe BNPs Synthesized by *Pleurotus ostreatus* Extract for (a) 60 min (b) effect of time (c) effect of concentration

ii.) Effect of Concentration:

As reflected in the UV spectrum represented the intensity of maximum absorption peak observed at 294 nm wavelength increases with an increasing concentration of $AgNO_3$ solution from 2 mM to 3 mM, the same also applies for FeNPs, the absorbance increases with concentration of $Fe(NO_3)_3$. But both cases, 1 mM concentration of salt is usually more effective than 2mM as the absorbance is higher in 1mM concentration of salt than 2 mM concentration.
For Ag-Fe BNPs the intensity of absorption in "a" (i.e 1mM of $AgNO_3$ and 2 mM of Fe $(NO_3)_3$ was lower than that of "b" (i.e 2 mM of $AgNO_3$ and 1mM of $Fe(NO_3)_3$. This suggests that the synthesis of Ag-FeBNPs can be optimized with the formal concentration.

ii. Effect of Ratio: The intensity of the UV absorption peak in ratio 1:2 of PO extract to salt solution was higher than that of ratio 1:3, hence ratio 1:2 is optimized for the synthesis.
The maximum absorption peak in the UV spectrum of Ag-Fe BNPs was observed at 248nm for ratio 1:1 of extract to precursor salt solution of $AgNO_3$ and Fe $(NO_3)_3$. This is similar to the study by Malik *et al*. 2021, where it was observed at 352nm when 1:1:1 of extract to precursor salt solution of AgNO3 and Fe (NO3)3 were used.

iv. Effect of pH: The UV spectrum of the PO extract showed different absorption peaks of different intensities for the acidic, neutral and alkaline pH as illustrated in Figure 3c. The spectrum with respect to the pH revealed an increasing intensity of absorption from acidic to alkaline extract which may be suggestive of an optimal green synthesis of the nanoparticles occurring more effectively using an acidic reducing agent since the increase in pH is inimical to the reductase capacity of phenolics present in the extract of the mushroom extract (Mandel and Hella, 2000).

FTIR Spectra of AgNPs and PO Extract: This was done to possibly identify likely biomolecules in *Pleurotus ostreatus* extract involved in the reduction, capping and stabilization of the synthesized nanoparticles. In Figure 4a, absorption bands were observed in the FT-IR spectrum of AgNPs at 472.77 cm-1, 617.45 cm^{-1}, 1039.4 cm^{-1}, 1082.06 cm^{-1} ,1119.8 cm-1,1237 cm^{-1}, 1384.78 cm^{-1}, 2308.7 $cm^{-1}$and 2345.6 cm^{-1}. The absorption bands at 472.77 cm^{-1},617.45 $cm^{-1}$are ascribed to =C-H bending of aromatics. The peaks at 1039.4 cm^{-1}, 1082.06 cm^{-1},1119.8 cm^{-1}, 1237 $cm^{-1}$and 1384.78 cm^{-1} are attributable to C-N stretching of amines while the bands at 2308.7 $cm^{-1}$and 2345.6 cm^{-1}may be assigned to O-H stretching of carboxylic acid.
The broad band observed between 3200 cm^{-1} and 3600 cm^{-1} is assigned to O-H stretching of alcohol and phenol, The FT-IR spectrum of *Pleurotus ostreatus* extract portrays a changes at a less intense peak of 2800 cm^{-1} which may be attributed majorly to C-H of an aldehyde and the consumption of peaks at 1600 cm^{-1} can be assigned majorly to C=C stretching of aldehydes, ketones and aromatics (Phenolics), that are found in flavonoids, phenolics, terpenes and lipid containing oils. The bands observed within 1000- 1140 cm^{-1} are attributed to carbonyl (C=O) stretching vibration of ketones while 1300 cm^{-1} and 1000 cm^{-1} band are assigned to C-N stretching in amine. Results of FTIR showed that the carbonyl assemblies from the residues of amino acid (protein) and phenolic acid has the more grounded capacity to bond metal, indicating that the proteins could shape the metal nanoparticles (i.e.; capping of silver nanoparticles) to counteract agglomeration and in this manner strongly balance out and alleviate the medium, hence the functional groups such as C–O and =C-O groups present in the sample might be responsible for bio reduction of Ag+ to AgNPs. This suggests that the natural biological atoms/molecules could act as stabilizing agents and formation of silver nanoparticles in the aqueous medium (Ejidike & Clayton, 2022).
Other bands observed are within 1000-1450 cm^{-1} range which experienced changes that showed the presence of carboxyl groups, expressing the involvement of these groups in the reduction and stabilization of the metal nanoparticle.

FTIR spectra of FeNPs and PO Extract: The following absorption peaks were identified in the FTIR spectrum of FeNPs: 473.22 cm^{-1} 532.01 cm^{-1}, 831.8 cm^{-1}, 1384.42 cm^{-1}, 1639.61 cm^{-1}, 2312 cm-1, 2345.6 $cm^{-1}$and 2925 cm^{-1} (Figure 4b). The observed absorption peaks at 473.22 cm-1, 532.01 cm^{-1}, 831.8 cm^{-1}may be assigned to =C-H bending of aromatics. Meanwhile the band at 1384.42 cm^{-1} is attributable to C-N stretching of amine and the peak at 1639.61 cm^{-1} corresponds to N-H bending of amine. The peaks observed at 2312 cm^{-1}, 2345.6 cm^{-1} and 2925 cm^{-1}were also assigned to the O-H stretching of carboxylic acid.
The FTIR spectra of FeNPs and Extract depicts a major change observed at 2932 cm^{-1} band reflecting consumption of a characteristic O-H stretching functional group carboxylic acid. The broad band between 3200 cm^{-1} and 3700 cm^{-1} were suggestive of alcohol or phenolic O-H stretching being involved in the reaction process. The major change at the peak observed in 1723.16 cm^{-1} is also confirming C=O stretching of carboxylic acid. Similarly, some observed differences in peaks at 1383 cm^{-1} and 1683 cm^{-1} band are attributable to C=C stretching of an aromatic ring of metabolites such as flavonoids and phenolic compounds. It can be concluded from these characteristic functional groups of O-H and C=O stretching of carboxylic acid and C=C stretching of aromatic ring that phenolic acid could be one of the biomolecules responsible for the reduction, capping and stabilizing of the FeNPs. Similar functional groups were reported in a study carried out by Faryal *et al*., 2021; Asif *et al*., 2022.

FTIR of Ag-Fe BMNPs and PO Extract: An FTIR analysis conducted (Figure 4c) to ascertain the organic molecules present in *Pleurotus ostreatus* which could be responsible for the reduction of Ag^+ and Fe^+ ions in the synthesis of nanoparticles showed various bands (559.43 cm^{-1}, 797.87 cm^{-1}, 908.82 cm^{-1}, 1040.18 cm^{-1}, 1076.3 cm^{-1},1234.59 cm^{-1}, 1384.30 cm^{-1},1538.4 cm^{-1},1639.32 cm^{-1}, 2343.77 cm^{-1}, 2851.3 cm^{-1}, 2925 cm^{-1}2958.4 cm^{-1}, 3417.60 cm^{-1}, 3632.12 cm^{-1} and 3679.04 cm^{-1}).
The bands at 3632.12 cm^{-1}, and 3679.04 cm^{-1} corresponds to hydroxyl group stretching (OH) of alkanol or phenol while

3417.60 cm^{-1} may be attributed to N-H stretching vibration of amine. Bands observed at 2343.77 cm^{-1}, 2851.3 cm^{-1}, 2925 cm^{-1}, 2958.4 cm^{-1}, are likely due to the O-H stretching of carboxylic acid. The bands at 1639.32 cm^{-1} region can be assigned to N-H bending of amine. 1384.30 cm^{-1} (strong) and 1538.4 cm^{-1} (medium) bands may be assigned to N=O vibration of Nitro (NO_2) group which may the due to impurities from the air. Bands at 1040.18 cm^{-1},1076.3 $cm^{-1}$and 1234.59 cm^{-1} are linked to C-N stretching of amine group while 559.43 cm^{-1}, 797.87 cm^{-1} and 908.82 cm^{-1} correspond to =C-H bending of aromatic ring (Dubey *et al*., 2024; Singh *et al*., 2025).

Presence of absorbance peaks in the carboxylic, hydroxyl, amine, group regions are particularly common in flavonoids, alkaloids, amino acids, fatty acids, and proteins/enzymes that have been reported for the reduction, capping and stabilizing of metal ions when using extract of fungi for the synthesis of metal nanoparticles. The result of the FTIR analysis investigated in this study, corresponds to a report of similar work by Mela *et al*, 2022. The major change in the peaks observed at 2933 cm^{-1} showed the consumption of O-H stretching of carboxylic acid.

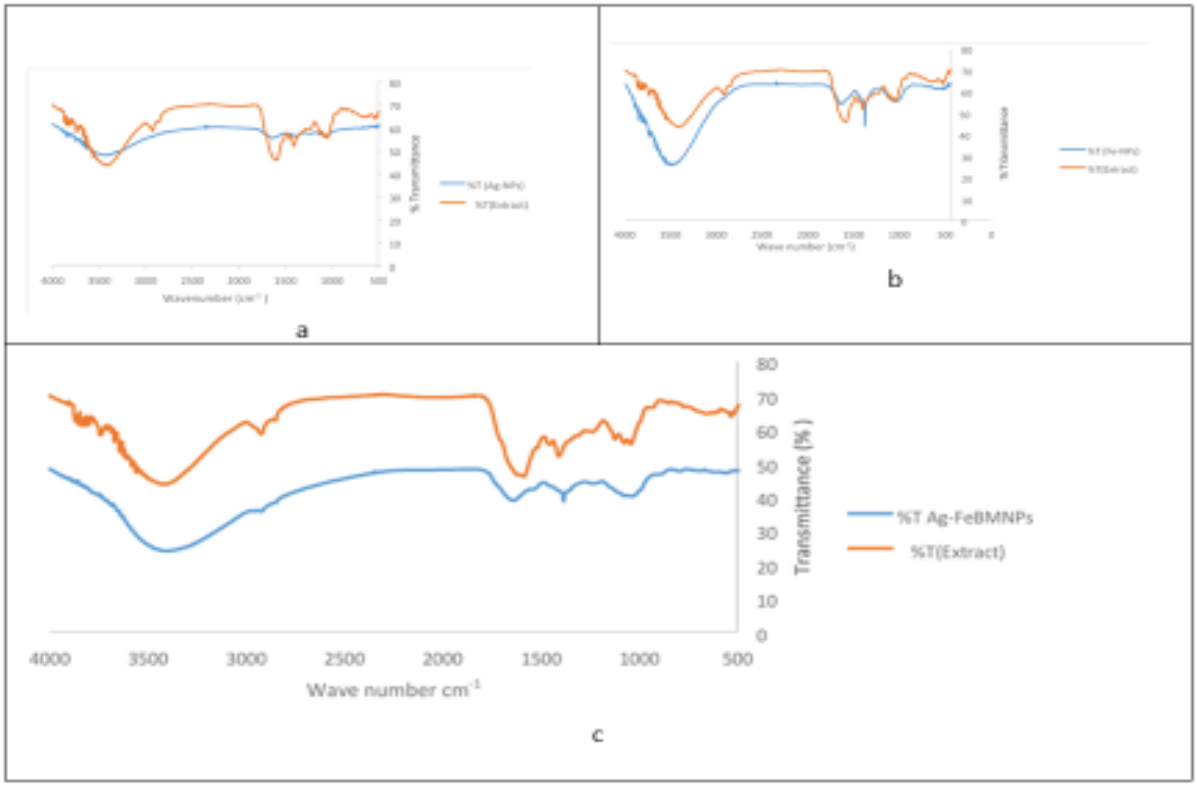

Figure 4:
FTIR spectrum of synthesized nanoparticles a) AgNNP (b) FeNNP (c) Ag-FeNNP

Scanning electron microscopy (SEM) of AgNPs, FeNPs, Ag-Fe BNPs: SEM image showing the morphological character of silver nanoparticles synthesis was observed (Figure 5a). Aggregation of the silver nanoparticles was observed with image sizes between 5 to 20 nm. Shapes which are spherical and rod shape with uniform distribution AgNPs on the surface of the cells clearly observed. The spherical shape-like morphology of most silver nanoparticles showed particle sizes ranging from 1 to 70 nm (Vanlalveni *et al*., 2021; Gohil *et al*., 2024)

The obtained SEM analysis result of the synthesized iron nanoparticles sample clearly showed that the Iron-NPs have a spherical shape with sizes in the range of 2-10 nm (Figure 5b) with agglomeration. Agglomerated iron nanoparticles are often observed in the powders obtained by co-precipitation.

The SEM of Ag-Fe bimetallic nanoparticles shows irregular clusters with rough surfaces, small agglomeration, and quasi-spherical in shape with a size of 5–20 nm. It showed well-capped and stabilized Ag-Fe bimetallic nanoparticles by the biomolecules present in the aqueous extract of the mushroom (Figure 5c).

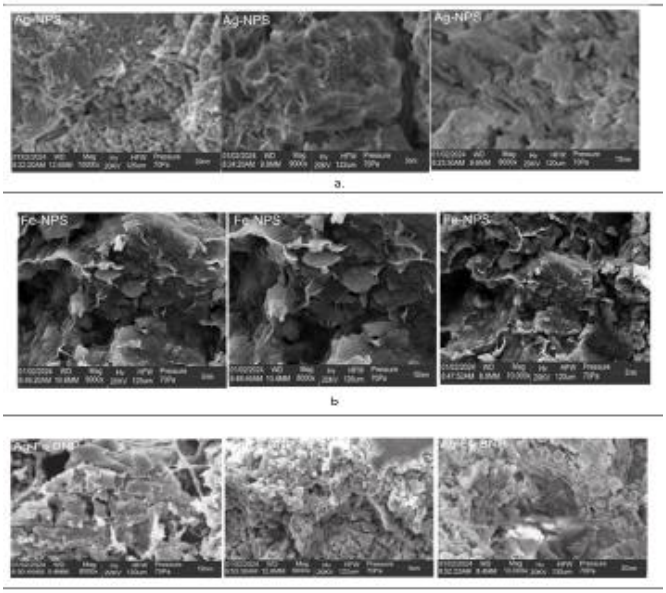

Figure 5:
SEM images of synthesized nanoparticles

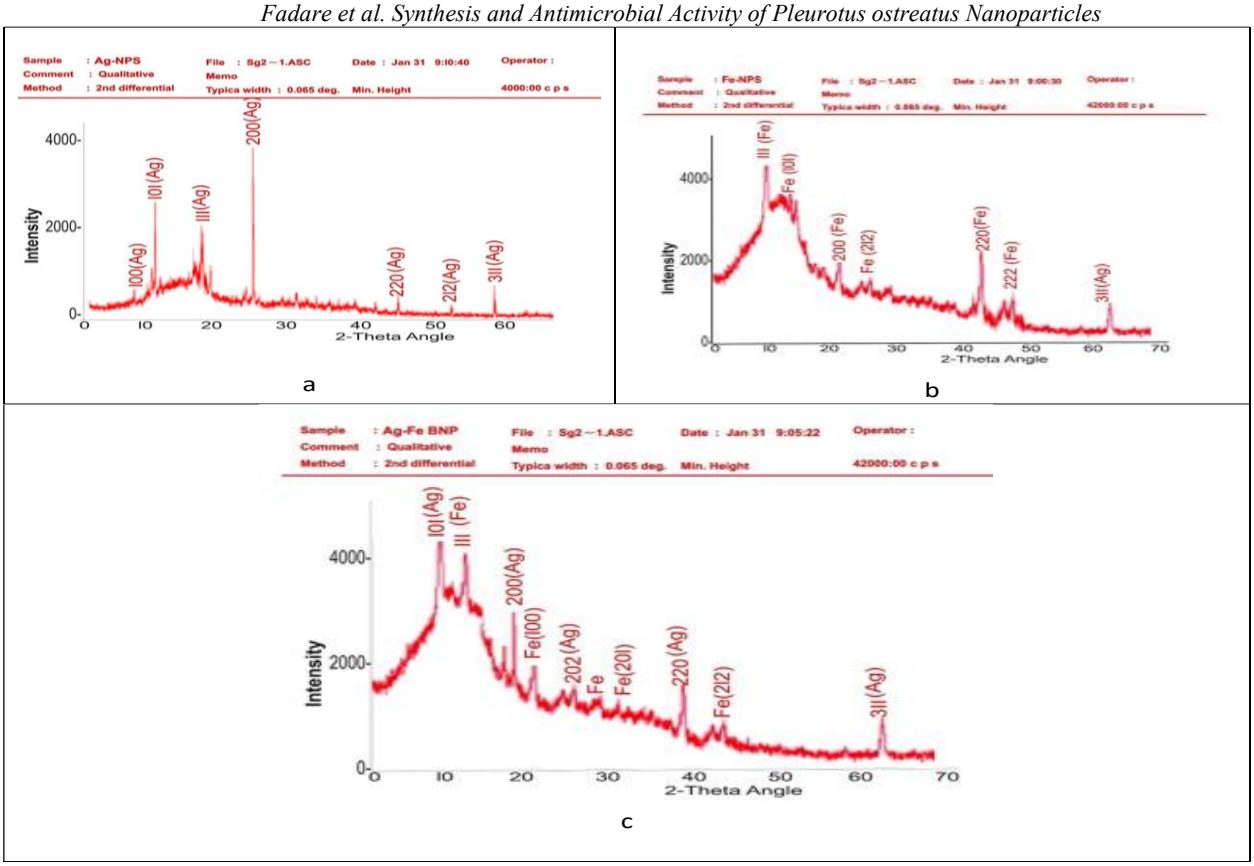

Figure 6:
XRD images of synthesized nanoparticles

X-ray Diffraction Analysis (XRD) of AgNPs, FeNPs, Ag-Fe BNPs: The diffracted intensities were recorded from 10 to 90 at 2 theta angles. The XRD patterns of Ag nanoparticles (Figure 6a) showed a crystalline structure (sharp peaks) with peaks at 2θ degrees of 38.17, 44.33, 64.53, 77.40, and 81.54, which can be attributed to the (111), (200), (220) and (311) crystalline planes of the face-centred cubic crystalline structure of metallic silver, respectively. This corresponds to the diffraction pattern of pure silver metal powder. Debye-Scherrer's equation was used to determine the average particle size of the AgNPs to be 46.7 nm.

Debye-Scherrer's equation: $D=K\lambda/b.\ Cos\theta$

Where reference u =peak width at angle, D= average grain size of crystallite, K = shape factor (0.98) λ = incident wavelength, and b = diffracted Full Width at Half Maximum.

The XRD pattern confirms the presence of Ag nanoparticles when prominent peaks were compared with literature with high intensity (20.313 and 48.089) and width of (110) plane at 2 =20.313 being narrow (Ogunsile *et al*. 2024).
The XRD pattern of the FeNPs peaks in Figure 6b were observed at a short range of 2θ of 10.20°(111), 12.25°(101), 20.45°(200), 25.05°(212), 42.44°(220), 49.50°(222) and 63.50 °(311).
The intensity at which the control sample crystalline face of the Fe Nano has a short range of 300–1500 cpu count compared to the Fe sample.
Figure 6 shows the XRD pattern of both Fe and Ag NPs powder. Fe peaks were observed at a 2θ of 10.33°-20.37°(101),12.24°-20.28°(111), 20.20°-23.22°(100), 30.47°22.44°(201), 44.05°(212), 25.44°(202), 38.50°(220) and 64.50 °(311); which matched with the crystal faces of the Ag Fe phase (101), (110), (111), (210), (211), (220) and (301), respectively, crystal planes, card 21-1272, JCPDS]. Peaks found at 2θ values of 14.42°, 29.62°, 44.48° and 64.75°; correspond to crystal planes of (101), (110), (111), (201) and (220) (Figure 6c) (Ogunsile *et al*., 2024).

Antimicrobial Activities of AgNPs, FeNPs and Ag-FeNPs: Antibacterial activities of the synthesized AgNPs, FeNPs, Ag-FeNPs and *Pleurotus ostreatus* are shown in Table 2. AgNPs showed the greatest activity of all the compounds tested. The most susceptible bacterium to AgNPs was *S. aureus*, with an inhibition zone diameter of 22mm, while Streptococcus p. was the most susceptible organism against Ag-Fe BNPs, with an inhibition zone diameter of 29 mm. FeNPs did not inhibit any of the bacteria at 100mg/cm but showed activity at higher doses. The synthesized AgNP has a better activity than the extracts, although there seems not to be any synergy in antibacterial activity in the bimetallic nanoparticle. (Naveed *et al*., 2022; Ogunsile *et al*, 2024).
In the antifungal assay, *Pleurotus ostreatus* extract demonstrated good antifungal efficacy, which corroborates the study of Elumalai et al., 2012 (Table 2). Of all the organisms tested, the yeast was the most susceptible to the nanoparticles. Zones of inhibition ranged from 7 mm to 24 mm with FeNPs demonstrating the highest antifungal activity.

Table 2: Antimicrobial activities of *Pleurotus ostreatus* extract and AgNPs, FeNPs and Ag-FeNPs

Test compounds (zone of inhibition, mm)													
Organisms	*Pleurotus ostreatus* (mg/mL)			AgNPs (mg/mL)			FeNPs (mg/cm^3)			Ag-Fe BNPs (mg/mL)			Gentamicin (10 mg)
	100	250	500	100	250	500	100	250	500	100	250	500	5
Bacteria													
K. pnemoniae	-	-	20	12	12	14	-	-	11	6	12	17	
S. aureus	-	-	18	11	18	22	-	7	12	-	-	4	
Streptococcus pnemoniae	-	-	24	10	16	19	-	7	15	17	18	29	
E. coli	-	-	16	13	14	16	-	-	15	-	-	-	
Fungi													Tioconazole 50 mg
P. notatum	10	15	25	-	-	15	12	15	22	-	-	-	50
A. niger	-	10	25	-	17	28	9	14	20	-	15	15	40
C. albicans	7	10	24	8	15	23	11	15	23	10	13	19	41

CONCLUSION

In this study, the biological synthesis of silver nanoparticles, iron nanoparticles and silver-iron bimetallic nanoparticles utilizing Oyster mushroom (PO) was shown to provide an ecological, well-disposed, simple, straightforward and effective route for the synthesis of considerate nanoparticles. For the producyion of oyster mushroom, substrate T4 with 73% sawdust, 25% corn cobs and 2% lime additive ranked first based on well-defined yield parameters. The UV-visible spectra of AgNPs, FeNPs and Ag-Fe BNPs showed maximum absorption 295 nm, 298 nm and 300 nm, respectively. The UV spectra of the nanoparticles showed that the intensities of the absorption peaks vary with time, concentration and ratio of extract to precursor salt solution. The synthesized nanoparticles in this study were mostly spherical with sizes between 2 and 20 nm. Silver nanoparticles have been found to demonstrate several theraupetic potentials including antimicrobial, antiplasmodial, larvicidal etc. The antimicrobial assay showed that the synthesized AgNNP demonstrated good activity. Research into development of stable nanoparticles for commercial use is recommended.

REFERENCES

Asif, M., Yasmin, R., Asif, R., Ambreen, A., Mustafa, M., & Umbreen, S. (2022). Green synthesis of silver nanoparticles (AgNPs), structural characterization, and their antibacterial potential. *Dose-response*, 20(2), 15593258221088709.

Banerjee, P., Satapathy, M., Mukhppahayay, A. and Das, P. 2014. Leaf extract mediated green synthesis of silver nanoparticles from widely available Indian plants: synthesis, characterization, antimicrobial property and toxicity analysis. *Bioresources and Bioprocessing-Springer Open Journal*. 1: 1-10

Basheer, M. A., Abutaleb, K., Abed, N. N., & Mekawey, A. A. (2023). Mycosynthesis of silver nanoparticles using marine fungi and their antimicrobial activity against pathogenic microorganisms. *Journal of Genetic Engineering and Biotechnology*, 21(1), 127.

Deepalakshmi, K., & Sankaran, M. (2014). *Pleurotus ostreatus*: an oyster mushroom with nutritional and medicinal properties. *Journal of Biochemical Technology*, 5(2), 718-726.

Dubey, S., Virmani, T., Yadav, S. K., Sharma, A., Kumar, G., & Alhalmi, A. (2024). Breaking barriers in eco-friendly synthesis of plant-mediated metal/metal oxide/bimetallic nanoparticles: antibacterial, anticancer, mechanism elucidation, and versatile utilizations. *Journal of Nanomaterials*, 2024(1), 9914079.

Ejidike, I. P., & Clayton, H. S. (2022). Green synthesis of silver nanoparticles mediated by Daucus carota L.: antiradical, antimicrobial potentials, in vitro cytotoxicity against brain glioblastoma cells. *Green Chemistry Letters and Reviews*, 15(2), 298-311.

Faryal, B., Muhammad, S., Salah-ud-din, K., Javed, K., Bilal, A. and Muhammad, I. 2021. Biologically synthesized iron nanoparticles (FeNPs) from Phoenix dactylifera have anti-bacterial activities. *Scientific reports*. 11: 22132.

Fasidi, I., Kadiri, M., Jonathan, S., Adenipekun, C. and Kuforiji, O. 2008. Cultivation of edible tropical mushrooms. Ibadan University Press. 1-25.

Fikre, T. 2012. Mushroom Production and Processing Technology (FSPT 422223). Hawassa, Ethiopia.

Francis, D. V., Jayakumar, M. N., Ahmad, H., & Gokhale, T. (2023). Antimicrobial activity of biogenic metal oxide nanoparticles and their synergistic effect on clinical pathogens. *International Journal of Molecular Sciences*, 24(12), 9998.

Gohil K, Dhakhda S, Patel V, Rathod A, Singh P. K. Green Synthesis of Silver Nanoparticles using Various Plant Extracts and Evaluation of their Antimicrobial Activities. *Biotech Res Asia* 2024;21(2).

Gour, A., & Jain, N. K. (2019). Advances in green synthesis of nanoparticles. *Artificial cells, nanomedicine, and biotechnology*, 47(1), 844-851.wsews

Hancharova, M., Halicka-Stępień, K., Dupla, A., Lesiak, A., Sołoducho, J., & Cabaj, J. (2024). Antimicrobial activity of metal-based nanoparticles: a mini-review. *Biometals*, 37(4), 773-801.

Itelima, J. U. (2012). Cultivation of mushroom (*Pleurotus ostreatus*) using corn cobs and saw dust as the major substrate. *Global Journal of Agricultural Sciences*, 11(1), 51-56.

Joudeh, N., & Linke, D. (2022). Nanoparticle classification, physicochemical properties, characterization, and

applications: a comprehensive review for biologists. *Journal of Nanobiotechnology*, 20(1), 262.

Keziah, S., Diana, S., Abdullah, A. and Ramwant, G. 2022. Effect of different organic substrates on growth and development of edible oyster mushroom (*Pleurotus ostreatus*). *Annals of Agricultural Science*. 43(4): 483-491.

Kumar, R., Kumar, S., Chandrappa, S. G., Goyal, N., Yadav, A., Ravishankar, N., ... & Sahoo, B. (2024). Nitrogen-doped carbon nanostructures embedded with Fe-Co-Cr alloy based nanoparticles as robust electrocatalysts for Zn-air batteries. *Journal of Alloys and Compounds*, 984, 173862.

Mandel, F. and Hella, S. J. 2000. Effect of pH on the stability of plant phenolics compounds. *Journal of Agric and Food Chemistry* .48(6): 2101-2110.

Manikanda, G. and Ramasubbu, R. 2021. Biosynthesis of Iron Nanoparticles from Pleurotus florida and its Antimicrobial Activity against Selected Human Pathogens. *Indian Journal of Pharmaceutical Sciences.* 83(1): 45-51.

Mc Wilson, O. D., & Del Rosario, A. B. (2020). Growth and yield of black oyster mushroom (*Pleurotus ostreatus*) on combined coconut sawdust and rice straw as lignocellulosic materials. *Agrik CRI* J, 3, 1-23.

Mohamed, Y., Azzam, A., Amin, B. and Safwat, N. 2015. Mycosynthesis of Iron Nanoparticles by Alternaria Altanata and its Antibacterial activity. *African Journal of Biotechnology*. 14 (14): 1234-1241.

Naveed, M., Bukhari, B., Aziz, T., Zaib, S., Mansoor, M. A., Khan, A. A., Shahzad, M., Dablool, A. S., Alruways, M. W., Almalki, A. A., Alamri, A. S., & Alhomrani, M. (2022). Green Synthesis of Silver Nanoparticles Using the Plant Extract of Acer oblongifolium and Study of Its Antibacterial and Antiproliferative Activity via Mathematical Approaches. *Molecules*, 27(13), 4226.

Oseni, T.O., Dube, S.S., Wahome, P.K., Masarirambi, M.T. and Earnshaw, D.M. 2012. Effect of Wheat Bran Supplement on Growth and Yield of Oyster Mushroom (*Pleurotus ostreatus*) on Fermented Pine Sawdust Substrate, Experimental Agriculture & Horticulture.

Padilla-Cruz, A., Garza-Cervantesl, J., Vasto-Anzaldo, X., Garcia-Rivas, G., León-Buitimea, A., and Morones-Ramirez, J. 2021. Synthesis and design of Ag—Fe bimetallic nanoparticles as antimicrobial synergistic combination therapies against clinically relevant pathogens. *Scientific Reports*. 11:5351 1

Paul, S., Sasikumar, C. S. and Singh, A. J. 2015. Fabrication of Silver Nanoparticles Synthesized from Ganoderma Lucidum into the Cotton Fabric and Its Antimicrobial Property. 7: 53-56.

Rambey,R., Sitepu, I.D. and Siregar, E.B. 2019. Productivity of oyster mushrooms (*Pleurotus ostreatus*) on media corncobs mixed with sawdust, TOP Conf. Series: Earth and Environmental Science. TOP Publishing. 260 012076.

Rawson, T. M., Ming, D., Ahmad, R., Moore, L. S., & Holmes, A. H. (2020). Antimicrobial use, drug-resistant infections and COVID-19. *Nature Reviews Microbiology*, 18(8), 409-410.

Ribeiro, A. I., Dias, A. M. and Zille, A. J. 2022. Synergistic Effects between Metal Nanoparticles and Commercial Antimicrobial Agents: A Review. 5: 3030-3064.

Saravanan, A., Kumar, P.S., Karishma, S., VO., Jeevanantham, S., Yaashikaa, P. and George, C. S. J. C. 2021. A review on biosynthesis of metal nanoparticles and its environmental applications. 264: 128-580.

Singh, R. K., Nallaswamy, D., Rajeshkumar, S., & Varghese, S. S. (2025). Green synthesis of silver nanoparticles using neem and turmeric extract and its antimicrobial activity of plant mediated silver nanoparticles. *Journal of Oral Biology and Craniofacial Research*, 15(2), 395-401.

Sneha, T. and Anisa, A. 2020. Biosynthesis of silver Nanoparticles using dried Agaricus bisporous edible mushroom and its antimicrobial activity against human pathogens. *International Journal of Engineering Applied Sciences and Technology*. 5(1): 763-767

Vanlalveni, C., Lallianrawna, S., Biswas, A., Selvaraj, M., Changmai, B., & Rokhum, S. L. (2021). Green synthesis of silver nanoparticles using plant extracts and their antimicrobial activities: A review of recent literature. *RSC advances*, 11(5), 2804-2837.

Ying, S., Guan, Z., Ofoegbu, P. C., Clubb, P., Rico, C., He, F., & Hong, J. (2022). Green synthesis of nanoparticles: Current developments and limitations. *Environmental Technology & Innovation*, 26, 102336.

Yoro, M., Samson, J. D., Joshua, J., Bello, P. D., & Jonah, J. W. K. (2022). Physicochemical parameters and antibacterial activity of biosynthesized silver nanoparticles from Carica papaya leaf extract. *Scholars International Journal of Chemistry and Materials Sciences,* 5(6), 105-110.

Zhuang, J. and Gentry, R. W. 2011. Environmental application and risks of nanotechnology: a balanced view, in Biotechnology and Nanotechnology Risk Assessment: Minding and Managing the Potential Threats around Us, eds. Washington, DC: *American Chemical Society Publications*. 41–67.

.